María L. Olivares[1,2]
Luciana Vera-Candioti[3]
Claudio L. A. Berli[1]

[1]INTEC (UNL-CONICET), Güemes, Santa Fe, Argentina
[2]Cátedra de Físicoquímica, FBCB, UNL, Ciudad Universitaria, Santa Fe, Argentina
[3]Cátedra de Química Analítica I, FBCB, UNL, Ciudad Universitaria, Santa Fe, Argentina

Received September 8, 2008
Revised October 24, 2008
Accepted November 12, 2008

Research Article

The EOF of polymer solutions

The EOF of polymer solutions is analysed in the framework of continuum fluid mechanics and the standard electrokinetic model. Two key aspects are taken into consideration: the non-Newtonian character of the fluid and the polymer concentration near the interface, which greatly modify the fluid viscosity in the region where electroosmosis takes place. A satisfactory mathematical model is derived for the electroosmotic mobility of solutions that present polymer depletion at the wall. The case of solutions containing polymers that adsorb onto the wall is briefly reviewed, and a preliminary approach is discussed for the limit of strong polymer adsorption. In order to illustrate the theoretical discussions, experimental data obtained from aqueous solutions of carboxymethyl cellulose in fused-silica capillaries are presented. Relevant results are observed, which are appropriately captured by the modelling proposed. The fundamental phenomena discussed in this work are of interest in microfluidics and electrophoresis.

Keywords:
EOF / Microfluidics / Non-Newtonian fluids / Polymer solutions
DOI 10.1002/elps.200800578

1 Introduction

Polymer solutions are widely used in CE, as well as in microfluidic devices. In these applications, fluids are transported by applying electric potential differences between channel ends, namely by EOF. For simple electrolyte solutions, the viscosity of which is a constant η_N (Newton coefficient), the electroosmotic mobility is given by the well-known Helmholtz–Smoluchowski (HS) equation,

$$\mu_{HS} = -\varepsilon\zeta/\eta_N \quad (1)$$

where ε is the electric permittivity and ζ is the electrokinetic potential [1–3]. Nevertheless, in the case of polymer solutions, the viscosity of which is a function of the velocity gradient developed in the microchannel (non-Newtonian behaviour), the electroosmotic mobility is expected to depend on the applied electric field [4].

Mathematical models of the EOF of non-Newtonian fluids are just emerging in the literature: Chakraborty [5] and Zhao *et al.* [6] considered the EOF of ''power law'' (PL) fluids in slit microchannels; Park and Lee [7, 8] calculated numerically the electroosmotic velocity of viscoelastic fluids in a square microchannel. It is relevant to note that all of these models implicitly assume that fluid properties are uniform in the whole domain, which in turn requires uniform polymer concentration throughout the flow field, including the interfacial region where electrokinetic effects take place. Nevertheless, such a situation is hardly found in experiments, as long as polymer solutions are considered. In fact, due to the unavoidable interaction between macromolecules and the channel surface, polymer concentration is altered in the proximity of channel walls. As a consequence, the solution viscosity changes considerably in the interfacial region in relation to the bulk fluid. The main phenomena to be considered are polymer depletion and polymer adsorption [9]. In the first case, one expects that the EOF of the polymer solution is equal to that of the pure solvent, because there are no macromolecules in the interfacial region [10, 11]. In the second case, the EOF is strongly diminished and even suppressed, as the viscosity of the fluid adjacent to the wall is significantly enhanced [12, 13]. Indeed, as the ζ-potential is also modified, polymer coating is the mechanism normally used to control the EOF in CE [14, 15].

In this context, the present work discusses the theoretical interpretation of the EOF of polymer solutions. For this purpose, the paper is organized as follows. Section 2 presents the governing equations of the fluid dynamic problem and briefly reviews the behaviour of polymers at interfaces. Section 3 discusses the mathematical modelling of the electroosmotic mobility for the cases of polymer adsorption and depletion. Section 4 describes the experiments carried out to measure the viscosity and electroosmotic mobility of a typical macromolecular solution. Section 5 analyses the modelling proposed in relation to experimental data and physicochemical characteristics of the system. Section 6 outlines the main conclusions.

Correspondence: Dr. Claudio L. A. Berli, INTEC (UNL-CONICET), Güemes 3450, Santa Fe 3000, Argentina
E-mail: cberli@santafe-conicet.gov.ar
Fax: +54-342-4550944

Abbreviations: CMC, carboxymethyl cellulose; **EDL,** electrical double layer; **HS,** Helmholtz–Smoluchowski; **PL,** power law

2 Theory

2.1 General considerations

The EOF is described in the framework of continuum fluid mechanics. Cylindrical microchannels of radius R and length L are considered, where the fluid velocity is established in the axial direction z and varies in the radial direction r. Temperature is assumed to be uniform throughout the flow domain, which requires negligible Joule effect in microchannels. In particular, here we include a non-Newtonian model for the viscosity of polymer solutions and take into account the concentration of polymers in the interfacial region.

Fluids presenting non-Newtonian behaviour necessarily contain discrete entities in their microstructure. In the case of polymer solutions, the size of these entities is characterized by the radius of gyration of macromolecules R_g, which may be several tenths of nanometres. In order to satisfy the continuum hypothesis, the present modelling requires $R_g \ll R$, a condition normally attained in micro-scale channels (typically $R > 10\,\mu m$). Further, in the case of electrically charged polymers, it is assumed that the possible electrophoretic effect does not influence the EOF.

2.2 Electric field and ion distributions

Electrokinetic effects depend on the existence of electrostatic charges in the solid–liquid interface [1, 2]. The interfacial charge has associated an electric potential $\psi(r)$ that decreases and vanishes in the fluid due to the screening produced by counterions and other electrolyte ions in the solution, which constitute the electrical double layer (EDL). There is also an externally applied potential $V(z)$ in the flow domain. Therefore, the total electric potential involves two contributions, $\Phi(r,z) = \psi(r) + V(z)$, and is governed by Poisson's equation, $\nabla^2\Phi(r,z) = -\rho_e/\varepsilon$. Here $\rho_e = e\sum_k \nu_k n_k$ is the electric charge density of the medium, which is obtained as the summation over all type-k ions with valence ν_k and number density n_k (e is the elementary charge). In particular, ion densities are considered to be uniform along the capillary, hence $\partial^2 V/\partial z^2 \approx 0$, which yields two relevant consequences: (i) the axial electric field $E = -\partial V/\partial z$ is uniform and (ii) the EDL potential is governed by

$$\frac{1}{r}\frac{\partial}{\partial r}\left(r\frac{\partial \psi}{\partial r}\right) = -\frac{\rho_e}{\varepsilon} \tag{2}$$

These assumptions are part of the standard electrokinetic model [1–3] and hold if $E \ll \zeta/\lambda$, which is normally the case in practice. In addition, taking into account that there is neither radial flux of ions nor flow in the radial direction, Nernst–Planck equations [1, 2] yield the Boltzmann-type distributions for the ionic species in the diffuse layer: $n_k = n_{b,k}\exp[-\nu_k e(\psi - \psi_b)/k_B T]$, where $n_{b,k}$ and ψ_b are, respectively, ion densities and electric potential in the bulk, k_B is the Boltzmann constant, and T is the absolute temperature. Therefore, the thickness of the EDL is given by the Debye length,

$$\lambda = \left(\varepsilon k_B T/e^2 \sum_k \nu_k^2 n_{b,k}\right)^{1/2}$$

2.3 Fluid velocity field

The steady-state flow of incompressible fluids in cylindrical capillaries of large aspect ratios ($L/R \gg 1$) is governed by the z-component of the momentum balance equation [1, 2, 16]:

$$\frac{\partial p}{\partial z} = \frac{1}{r}\frac{\partial (r\sigma_{rz})}{\partial r} + \rho g_z - \rho_e \frac{\partial V}{\partial z} \tag{3}$$

In this expression, p is the isotropic pressure, σ_{rz} is the shear component of the stress tensor, ρ is the fluid density, and g_z is the z-component of gravitational acceleration. Further, the last term on the right-hand side of Eq. (3) represents the contribution of electric forces due to the presence of the applied potential V. These forces manifest in the interfacial region where ρ_e is non-null, giving rise to the EOF, as considered in the standard electrokinetic model [1–3].

2.4 Viscosity model

In order to asses the velocity profile $u_z(r)$ of polymer solutions, a constitutive relationship for the shear stress σ_{rz} must be included in Eq. (3). The present modelling involves steady state, isothermal, fully developed, rectilinear shear flows, which fulfil the requirements of viscometric flow [16]. Under these conditions, the fluid viscosity η is defined to be a function of the shear rate $\dot{\gamma} = |\dot{\gamma}_{rz}|$, where $\dot{\gamma}_{rz} = \partial u_z/\partial r$ is the fluid velocity gradient. Therefore, by analogy to the empirical law of Newton ($\sigma_{rz} = \eta_N \dot{\gamma}_{rz}$, where η_N is a constant coefficient), one may introduce $\sigma_{rz} = \eta(\dot{\gamma})\dot{\gamma}_{rz}$, where the function $\eta(\dot{\gamma})$ describes the non-Newtonian viscosity of the inelastic fluid [16]. In particular, the PL model of Oswald-de Waele is expressed as $\eta(\dot{\gamma}) = \beta\dot{\gamma}^{\alpha-1}$, where α is the flow behaviour index and β is the consistency parameter [2, 16]. In fact, this model predicts a PL relation between η and $\dot{\gamma}$, and it is normally valid for relatively high shear rates, as those developed in microchannels. Values of $\alpha < 1$ indicate shear-thinning behaviour: η decreases with $\dot{\gamma}$, the most common response observed in polymeric fluids such as carboxymethyl cellulose(CMC) and poly-acrylamide solutions. On the other hand, $\alpha > 1$ indicates shear-thickening behaviour: η increases with $\dot{\gamma}$. When $\alpha = 1$, the Newton law is recovered with $\beta = \eta_N$. Parameters α and β strongly depend on polymer concentration and temperature [16]. In shear-thinning solutions, α decreases and β increases with polymer concentration.

The shear stress of PL fluids is then given by

$$\sigma_{rz} = \beta\dot{\gamma}^{\alpha-1}\dot{\gamma}_{rz} \quad (4)$$

This constitutive relation is very helpful because it properly represents practical situations and, at the same time, is sufficiently simple to allow analytical solutions of the EOF in capillaries. More sophisticated $\eta(\dot{\gamma})$ functions demand numerical calculations to extract $u_z(r)$. Nevertheless, it is worth remarking that the PL model cannot describe time-dependent responses or viscoelastic phenomena. In this sense, it should be noted that elastic effects take relevance in systems that present contractions/expansions, curves, and mainly, unsteady flows, whereas this modelling is concerned with steady-state flow in straight microchannels.

2.5 Polymers at the interface

Polymer solutions presenting non-Newtonian behaviour involve macromolecules with relatively high molecular weight, the size of which are several tenths of nanometres, whereas the thickness λ of the EDL associated with the wall is normally lower than 10 nm. Therefore, the distribution of macromolecules at the interface cannot be ignored in modelling the EOF of polymer solutions. In what follows, we discuss the limiting situations, always considering smooth surfaces.

2.5.1 Polymer adsorption

If the interaction between macromolecules and the surface is attractive, macromolecules adhere to the wall [9, 17–20]; hence the polymer segment concentration $\phi(r)$ increases abruptly near the surface (Fig. 1A). This behaviour is observed for neutral and charged polymers. In particular, a wide class of macromolecules adsorb onto silica surfaces, mainly those that are capable of forming hydrogen bonds with OH-groups exposed at the surface [22]. The extent of the adsorption depends on the pH of the medium, ionic strength, polymer concentration, and temperature. In general, electroosmosis is strongly diminished due to the fact that polymer concentration in the interfacial region is much higher than that in the bulk (Fig. 1A), and consequently the viscosity of the fluid adjacent to the wall increases significantly [4, 12, 13]. Another crucial aspect is that polymer coating modifies the magnitude of the ζ-potential, and even the sign, depending on the electrical charge of polymers [3, 14, 15].

2.5.2 Polymer depletion

If the interaction between macromolecules and the surface is repulsive, the polymer segment concentration decreases steeply near the surface (Fig. 1B), which yields a depletion layer adjacent to the wall [9, 17, 18]. In particular, if the polymer concentration vanishes ($\phi_w = 0$ in Fig. 1B), the fluid in the depletion layer is the solvent of the polymer solution. The main consequence of this phenomenon is that the viscosity of the depletion layer is much lower than that of the bulk, which leads to the apparent hydrodynamic slip observed in polymer solutions [21, 23], as well as in a variety of colloidal systems (see [24] for a comprehensive review on the subject). A second relevant aspect of polymer depletion is that the ζ-potential is not altered by the presence of the polymer, except for the possible changes in the ionic strength of the medium. In fact, as polymers never touch

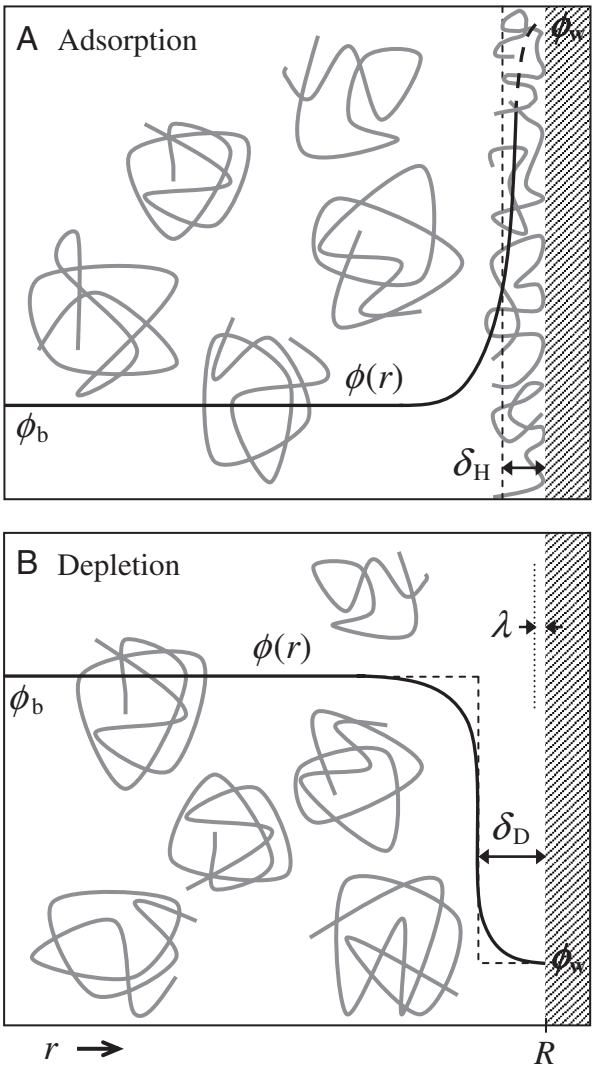

Figure 1. Highly schematic representation of polymers in the proximity of an interface, showing the occurrence of (A) adsorption and (B) depletion. In both cases, the curve $\phi(r)$ represents the polymer segment concentration, where ϕ_b and ϕ_w are the values in the bulk solution and at the wall, respectively (arbitrary drawings following [9, 18]). The departure of $\phi(r)$ from ϕ_b occurs at a distance from the wall that corresponds to the characteristic correlation length in semi-dilute solutions, or the radius of gyration of macromolecules in dilute solutions [9, 18, 19, 21]. In (A), δ_H is the hydrodynamic thickness of the adsorbed layer. In (B), δ_D is the width of the depletion layer and λ is the EDL thickness (not to scale).

the wall, in principle, the EDL associated with the channel surface is not distorted.

3 Modelling the EOF

3.1 Uniform polymer concentration

Firstly we discuss non-Newtonian effects alone. Hence the virtual situation in which polymer concentration is not modified near the wall (not shown in Fig. 1) is considered:

$$\phi(r) = \phi_b, \quad 0 \le r \le R \tag{5}$$

Therefore, Eq. (3) is valid in the whole flow domain, including the region of the EDL. Mathematical derivations are carried out in Appendix A. The electroosmotic velocity $u_U^{(e)}$ is given by Eq. (A7), from which the mobility $\mu_U = u_U^{(e)}/E$ results

$$\mu_U = \alpha\left(-\frac{\varepsilon\zeta}{\beta}\right)^{1/\alpha}\left(\frac{E}{\lambda}\right)^{1/\alpha-1} \tag{6}$$

This functionality has been obtained by Bello *et al.* [4] from scaling relations, although without the exact numerical factors.

Equation (6) equals Eq. (1) when $\alpha = 1$ and $\beta = \eta_N$ (Newtonian fluid). In contrast, for arbitrary values of α, Eq. (6) presents three main features in comparison with the HS equation: (i) μ_U depends on the applied electric field, due to the coupling of electrokinetic and non-Newtonian phenomena. The effect is illustrated in Fig. 2. (ii) μ_U depends on the Debye length. The physical meaning of this result can be understood by considering that the fluid viscosity is a function of the velocity gradient $\partial u_z/\partial r$, which directly depends on the EDL thickness λ. This is another manifestation of the coupling between electrokinetic and non-Newtonian phenomena. (iii) μ_U is non-linear with the surface potential. It must be noted here that ζ is also related to λ, as both depend on the ionic strength of the medium. In this sense, Eq. (6) has to be connected to a theoretical expression giving ζ in terms of λ for the system in consideration [25]. Simplified relations $\zeta(\lambda)$ may be used as well [26].

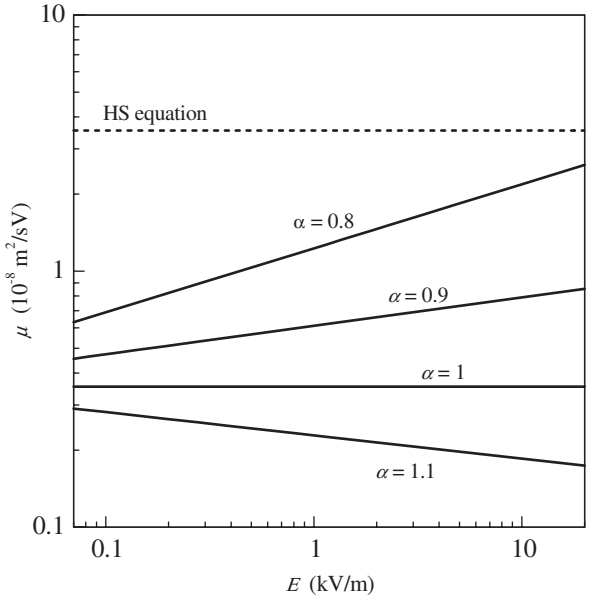

Figure 2. Electroosmotic mobility as a function of the applied electric field, according to Eq. (6) (uniform polymer concentration). Solid lines represent polymer solutions with $\beta = 0.01\ \text{Pas}^{\alpha}$ and different flow indexes α. Other parameter values used in calculations are $\varepsilon = 7.1 \times 10^{-10}\ \text{C}^2/\text{Nm}^2$, $\zeta = -50\ \text{mV}$, $\lambda = 10\ \text{nm}$. The dotted line represents an electrolyte solution with the viscosity of water (Eq. (1); $\eta_N = 0.001\ \text{Pas}$), which is included for comparison. In particular, the curve with $\alpha = 1$ represents a Newtonian polymer solution with viscosity ten times higher than that of water.

3.2 Polymer adsorption

3.2.1 General case

The effects predicted by Eq. (6) are due to the fact that, at a given polymer concentration, the fluid viscosity depends on the shear rate. When polymer adsorption takes place, the viscosity will also change locally due to the variation in polymer concentration near the surface (Fig. 1A). If one rationalizes the problem in the context of the PL model, the first aspect to remark is that parameters α and β are no longer constant in the vicinity of the wall, as they depend on polymer concentration [16]. In addition, whether a plane of shear with the associated ζ-potential can be defined in the interfacial region is questionable, as required to apply the standard electrokinetic model [3].

In fact, the overall consequences of polymer adsorption on electroosmosis were predicted by Hjertén 40 years ago, as described in [12]. Nevertheless, to the best of our knowledge, theoretical descriptions of the EOF taking into account the viscosity variation near the wall have not been reported to present, with the exception of the work of Otevřel and Klepárník [27], who considered Newtonian fluids and made no inferences on the plane of shear. Many efforts have been made, however, to describe the surface potential after analytes adsorption from dilute solutions [28–33]. On the other hand, models addressed to describe electrokinetic phenomena in polymer-coated surfaces also involve simple electrolyte solutions [34–36]. Evidently, modelling the full problem demands additional investigation. Below we restrict our analysis to the limit of strong adsorption ($\phi_w \gg \phi_b$; Fig. 1A), where a simplified picture of the interface may be assumed.

3.2.2 Strong adsorption

Let us consider the situation in which the attractive interaction energy between polymers and the surface is higher than the thermal energy k_BT [17], so that the adhered macromolecules form a compact, non-draining, solid-like

layer. Silica surfaces are particularly susceptible to such a strong polymer adsorption [22]. Robust and stable coatings are also achieved by using successive multiple ionic layers [37]. According to [34–36], the non-draining condition means a relatively large frictional factor for the solvent inside the polymer layer. According to [27], the solid-like condition means that the fluid viscosity in the adsorption layer is much higher than that of the central zone. Under these conditions, the flow will develop out of the adsorbed layer, for $r < R-\delta_H$, where δ_H is the hydrodynamic thickness of the adsorbed layer. Thus the channel has an effective radius equal to $R-\delta_H$ (Fig. 1A, dashed line), and the plane of shear is placed on the new interface, which satisfies

$$r = R - \delta_H, \quad u_z = 0, \quad \psi = \zeta_{eff} \tag{7}$$

Obviously the existence of an effective surface potential ζ_{eff} onto the adsorbed layer is essential for the development of EOF. Moreover, ζ_{eff} should be uniform throughout the interface [28–33].

If polymer concentration obeys $\phi(r) = \phi_b$, $0 \leq r \leq R - \delta_H$, one may take advantage of the procedure described in Appendix A, with the new boundary condition. In fact, by using Eq. (7) instead of Eq. (A3), calculations reproduce Eq. (6) with ζ_{eff} instead of ζ. This simple result is reasonable for the ideal interface conjectured above. It should be noted that the mobility does not depend on δ_H, which is in agreement with the results reported in [37]: given a compact coating, the magnitude of the EOF is defined by the resulting surface potential, and does not vary appreciably with the thickness of the adsorbed layer. However, concerning ζ_{eff}, it is known that determining the electrokinetic potential of polymer covered surfaces is full of difficulties, and the physical interpretation of measured values is sometimes ambiguous (for detailed discussions on the subject see [3] and references therein).

3.3 Polymer depletion

This section deals with systems in which polymer concentration decreases near the wall, as shown in Fig. 1B. In order to describe the EOF, firstly we approximate $\phi(r)$ by a step-like function (Fig. 1B, dashed lines) as follows:

$$\phi(r) = \begin{cases} \phi_b, & 0 \leq r \leq R - \delta_D \\ \phi_w, & R - \delta_D < r \leq R \end{cases} \tag{8}$$

Then we split the flow domain in two parts: the bulk fluid and the depletion layer, respectively. It is supposed that the fluid obeys the PL model in both regions, but with different parameter values. The parameters of the bulk polymer solution are those assessed by rheometry (α and β, as before), whereas those in the depletion layer (α_D and β_D) are in principle unknown. Nevertheless, one may infer that $\alpha_D > \alpha$ and $\beta_D < \beta$, taking into consideration the fact that both the shear-thinning degree and viscosity level of polymer solutions decrease with polymer concentration [16].

The plane of shear is assumed to be placed on the wall (see also Section 2.5.2). We further consider that the EDL potential is completely screened in the depletion layer, taking into account that, for the ionic concentrations normally used in practice, λ is rather lower than δ_D, which is on the order of the radius of gyration of macromolecules. The mathematical problem is formulated and solved in Appendix B. The electroosmotic velocity $u_D^{(e)}$ is given by Eq. (B7), from which the mobility $\mu_D = u_D^{(e)}/E$ results

$$\mu_D = \alpha_D \left(-\frac{\varepsilon\zeta}{\beta_D}\right)^{1/\alpha_D} \left(\frac{E}{\lambda}\right)^{1/\alpha_D - 1} \tag{9}$$

It is observed that μ_D depends on the fluid characteristics of the depletion layer alone, *i.e.* electroosmosis is unrelated to the bulk fluid. Further, μ_D is independent of the thickness δ_D, a result valid for pure EOF (no pressure gradients), and thin EDL ($\lambda \ll \delta_D$).

In the case of strong depletion, the polymer segment concentration vanishes at the wall, that is, $\phi_w = 0$ in Eq. (8) (see also Fig. 1B). Consequently, the depletion layer is filled with the solvent of the polymer solution, which is normally a Newtonian fluid. Therefore the electroosmotic mobility is simply obtained by substituting $\alpha_D = 1$ and $\beta_D = \eta_N$ into Eq. (9), which yields Eq. (1). Then the EOF is described by the linear HS equation, regardless of the non-Newtonian character of the bulk polymer solution. In fact, the interesting feature of strong depletion is that the EOF is not coupled to non-Newtonian effects, because electroosmosis is confined to the region of pure solvent adjacent to the wall. The electrokinetic flow of colloidal systems that exhibit wall depletion has been thoroughly studied in a previous work [11].

4 Materials and methods

In order to illustrate the theoretical predictions, this work includes experiments carried out with aqueous solutions of CMC, which is a natural polymer widely employed in industrial applications such as food and pharmaceutics. More specifically, it is used in CE as a chiral selector [38]. The physicochemical characteristics of the polymer [39] as well as its ability to adsorb on hydrophilic surfaces [40] are known. The rheological properties of aqueous solutions of CMC are also available [41]. In what follows, we present the materials and methods used in our research.

4.1 BGE and polymer solutions

Distilled water was used for preparing all the solutions. Sodium diacid phosphate 15 mM solution was used as the buffer, pH 7, hereafter called the BGE. Urea 5 M was added to some solutions. High-viscosity-grade CMC (sodium salt, item 6331 from Anedra S.A., Argentina) was used. Aqueous solutions of CMC were prepared as follows. First the CMC powder was subjected to hydration in the BGE for 15 min.

Then the hydrated powder was dissolved in a volume of buffer near that required to reach 1% w/v. Magnetic stirring was applied for 1 h at room temperature. The pH was adjusted to 7 and the final volume was reached. Finally CMC solutions were filtered through a 0.45-μm nylon membrane (Sartorius, Germany) and degassed in an ultrasonic bath before use.

4.2 Physicochemical characteristics

CMC is a long-chain polysaccharide that is negatively charged at pH 7 [39]. The average molecular mass of CMC may be estimated from viscosity data in the low shear rate regime, by using a well-defined relationship reported in [41]. Considering that the viscosity of 1% CMC solutions was 0.37 Pas at $\dot{\gamma} = 1\,s^{-1}$, the average molecular mass of our samples is around 500 kg/mol. Following [39], this value corresponds to a radius of gyration of approximately 150 nm (naturally, these samples are expected to be rather polydisperse in size). The Debye length of BGE is $\lambda \approx 3.5$ nm, whereas that of CMC solutions is around 1 nm, or less, because of sodium ions from CMC molecules.

4.3 Rheological measurements

The viscosity function $\eta(\dot{\gamma})$ of CMC solutions was determined on a stress-controlled rheometer (Haake RheoStress RS80, Haake Instrument, Paramus, NJ, USA), by using a cone-plate cell with the following characteristics: cone radius, 3 cm; cone angle, 1°; sample volume, 1 mL. The viscosity η was measured at different shear rates $\dot{\gamma}$ between 1 and 1000 s^{-1}, while the temperature was kept constant at 25°C. Experimental runs were repeated three times.

4.4 EOF measurement

The electroosmotic mobility of different solutions was determined on a CE instrument (Agilent Technologies, Waldbronn, Germany), by using uncoated fused-silica capillary tubes (Microsolv, USA) with the following characteristics: total length $L = 38$ cm, effective length $L_{eff} = 29.5$ cm, inner diameter $2R = 75$ μm. The capillary, when new, was washed successively with filtered 1 M sodium hydroxide solution, with 0.1 M sodium hydroxide solution, with Milli-Q water (Millipore, USA) and with BGE, for 10 min each one. At the beginning of the working day, the capillary was washed with sodium hydroxide 0.1 M solution, Milli-Q water and finally with BGE for 10 min. Between runs, the capillary was washed with BGE for 3 min. The cartridge was thermostated at 25°C. Detection wavelength was fixed at 245 nm. EOF velocity was measured by employing acetone as a neutral marker, which was injected by pressure (30 mbar, 10 s). In each run, the migration time t_m of the marker to the detector was recorded. Then the experimental mobility was calculated as $\mu_{exp} = L_{eff}/(t_m E)$, where $E = \Delta V/L$, being ΔV the electric potential difference applied between capillary ends. The maximum ΔV used was 10 kV in order to avoid Joule heating in the capillary. Experimental runs were repeated five times.

5 Results and discussion

Figure 3 presents a typical viscosity curve of CMC solutions obtained by cone-plate rheometry. Viscosity values are around two orders of magnitude higher than that of the BGE (0.001 Pas), and a strong shear-thinning behaviour is observed. In particular, CMC solutions present a PL region for $\dot{\gamma} > 200\,s^{-1}$, approximately. This behaviour is described by the straight line in Fig. 3, the slope of which is $\alpha - 1$, and the intercepts at $\dot{\gamma} = 1\,s^{-1}$ is β (parameter values are reported in the figure). The whole curve of experimental data, including the region of low shear rates, is well described by Carreau model [41]. Nevertheless, this work is concerned with the EOF, which involves the high shear rate region, where CMC solutions evidently behave as PL fluids.

Figure 4 presents typical results of the electroosmotic mobility of CMC solutions in fused-silica capillaries. First, it is appropriate to mention that the dotted line is the prediction of Eq. (1), which represents the mobility of the BGE (triangles), while the solid line is the prediction of Eq. (6) with parameters α and β obtained by rheometry. It is observed that experimental data of the CMC solution (Fig. 4, diamonds) fall in an intermediate position, with mobility values about 20% lower than those of the BGE. This behaviour coincides with results reported by Bello *et al.* [4] from aqueous solutions of methyl

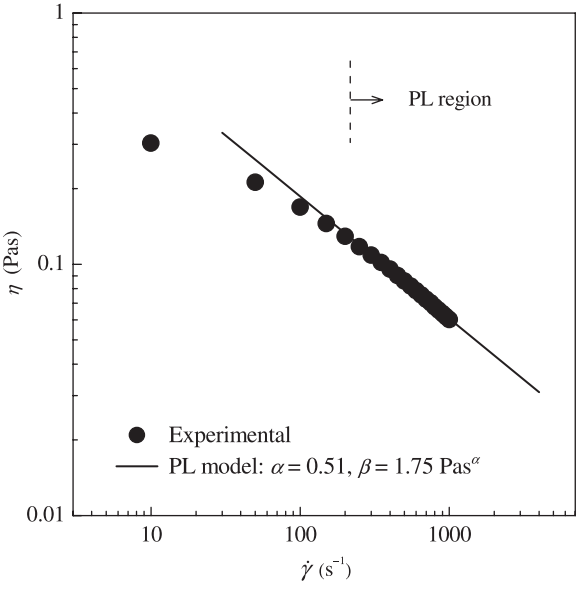

Figure 3. Viscosity as a function of shear rate for 1% CMC solutions (pH 7; 25°C). Symbols are experimental data obtained by rheometry. The line is the prediction of the PL model ($\eta(\dot{\gamma}) = \beta\dot{\gamma}^{\alpha-1}$) with the parameter values indicated into the graphic, which are valid for $\dot{\gamma} > 200\,s^{-1}$.

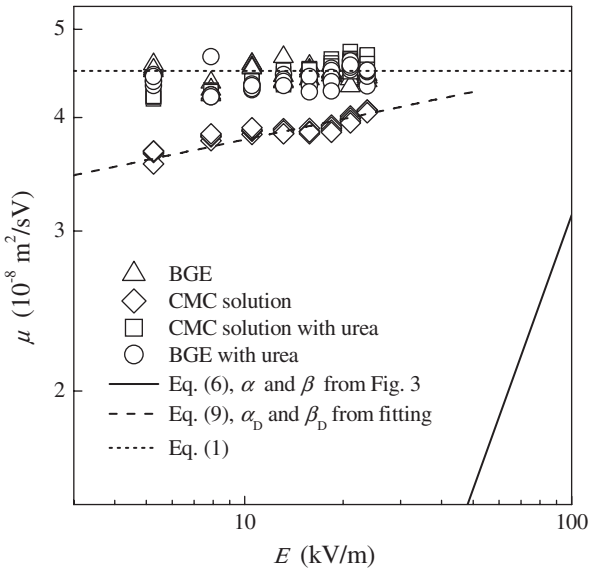

Figure 4. Electroosmotic mobility as a function of the applied electric field. Symbols are experimental results obtained with 1% CMC solutions in fused-silica capillaries (pH 7; 25°C). Lines are the prediction of the different models described in Section 3, with $\varepsilon = 7.1 \times 10^{-10}\,C^2/Nm^2$ and $\zeta = -60$ mV. Other parameter values used in calculations are: Eq. (6), $\alpha = 0.51$, $\beta = 1.75\,Pas^{\alpha}$, $\lambda = 1$ nm; Eq. (9), $\alpha_D = 0.93$, $\beta_D = 0.0026\,Pas^{\alpha}$, $\lambda = 1$ nm; Eq. (1), $\eta_N = 0.001$ Pas.

cellulose in fused-silica capillaries. At this step of the analysis, one may conclude that CMC solutions neither present uniform polymer concentration in the interfacial region, as required to follow the prediction of Eq. (6), nor exhibit strong depletion, as required to follow the prediction of Eq. (1).

It is also observed in Fig. 4 that mobility data of the CMC solution follow a PL relation, with a relatively low degree of shear-thinning. According to the theoretical discussions given in Section 3.3.1, this result suggests the occurrence of polymer depletion. In fact, a straightforward fitting with Eq. (9) (dashed line) yields $\alpha_D = 0.93$, which is notably higher than the value of α obtained by rheometry (Fig. 3). If one further considers that $\zeta \approx -60$ mV and $\lambda \approx 1$ nm, then $\beta_D \approx 0.0026\,Pa\,s^{\alpha}$, which is much lower than β obtained by rheometry (Fig. 3).

When urea is added to the CMC solution, the resulting EOF (Fig. 4, squares) is equivalent to that of the BGE. This remarkable result indicates that strong depletion of polymers takes place now. Indeed, it is known that urea inhibits the formation of hydrogen bonds between CMC molecules and the silica surface, which is the main mechanism for CMC adsorption [22, 40]. Therefore, the weak concentration of polymers in the depletion layer (without urea) could be due to certain degree of CMC adsorption. Experimental data of BGE with urea are included in Fig. 4 to show that urea does not alter appreciably neither the viscosity nor the surface potential.

From a physicochemical point of view, we may argue that a polymer concentration profile similar to that depicted in Fig. 1B, with $\phi_w \ll \phi_b$, is highly possible in the system without urea: CMC molecules are negatively charged at pH 7, as well as the capillary surface; thus depletion occurs due to electrostatic repulsion. Nevertheless, even in this unfavourable situation, CMC is able to adsorb onto hydrophilic surfaces by forming hydrogen bonds [22, 40], which gives $\phi_w > 0$. Under the circumstances, the fluid in the interfacial region results more viscous than the BGE, but less viscous and less shear-thinning than the bulk solution. Then Eq. (9) applies satisfactorily, taking into account that δ_D ($\sim$150 nm) is rather higher than λ ($\sim$1 nm). Finally, the effect of urea consists in shifting $\phi_w \to 0$, leading to a fully depleted layer with Newtonian viscosity, which is interpreted by Eq. (1).

6 Concluding remarks

In this work we analyse the EOF of polymer solutions taking into consideration two main aspects: the non-Newtonian character of the fluid and the polymer concentration profile near the interface where electroosmosis takes place. The EOF of solutions with uniform polymer concentration is analysed first in order to discuss the non-linear effects associated with the non-Newtonian viscosity.

A satisfactory mathematical model is derived for the EOF of solutions that present polymer depletion at the wall. In the limit of strong depletion, which is common in colloids, the electroosmotic velocity is linear and given by HS equation.

The case of solutions containing adsorbing polymers is also reviewed, and a simple approach is suggested for the limit of strong polymer adsorption. Further efforts are required to model the general problem, and a comprehensive experimental program is needed for the purposes. This topic will be considered in future works.

The experiments carried out here illustrate the main concern expressed in our theoretical discussion: the viscosity function obtained by rheometry (bulk property) should not be used to quantify the EOF (interfacial phenomena) without any further consideration. In particular, for CMC solutions, one observes that both polymer depletion and a certain degree of specific adsorption contribute to define the electroosmotic mobility.

One may finally remark that the concepts discussed throughout this work are of interest in microfluidics, as well as in several electrophoretic techniques.

The authors thank Agencia Nacional de Promoción Científica y Tecnológica (ANPCyT) and Consejo Nacional de Investigaciones Científicas y Técnicas (CONICET), Argentina, for the financial aid received.

The authors have declared no conflict of interest.

7 References

[1] Probstein, R. F., *Physicochemical Hydrodynamics*, Butterworths, New York 1989.

[2] Hunter, R. J., *Foundations of Colloid Science*, vols. I and II, Clarendon Press, Oxford 1992.

[3] Delgado, A. V., González-Caballero, F., Hunter, R. J., Koopal, L. K., Lyklema, J., *(IUPAC Technical Report) J. Colloid Interface Sci.* 2007, *309*, 194–224.

[4] Bello, M. S., de Besi, P., Rezzonico, R., Righetti, P. G., Casiraghi, E., *Electrophoresis* 1994, *15*, 623–626.

[5] Chakraborty, S., *Anal. Chim. Acta* 2007, *605*, 175–184.

[6] Zhao, C., Zholkovskij, E., Masliyah, J. A., Yang C., *J. Colloid Interface Sci.*, 2008, doi: 10.1016/J.Jcis.2008.06.028.

[7] Park, H. M., Lee, W. M., *J. Colloid Interface Sci.* 2008, *317*, 631–636.

[8] Park, H. M., Lee, W. M., *Lab Chip,* 2008, *8*, 1163–1170.

[9] de Gennes, P.-G., *Adv. Colloid Interface Sci.* 1987, *27*, 189–209.

[10] Zimmerman, W. B., Rees, J. M., Craven, T. J., *Microfluid. Nanofluid.* 2006, *2*, 481–492.

[11] Berli, C. L. A., Olivares, M. L., *J. Colloid Interface Sci.* 2008, *320*, 582–589.

[12] Hjertén, S., *J. Chromatogr.* 1985, *347*, 191–198.

[13] Mazzeo, J. R., Krull, I. S., *Anal. Chem.* 1991, *63*, 2852–2857.

[14] Righetti, P. G., Gelfi, C., Verzola, B., Castelletti, L., *Electrophoresis* 2001, *22*, 603–611.

[15] Danger, G., Ramonda, M., Cottet, H., *Electrophoresis* 2007, *28*, 925–931.

[16] Bird, R. B., Armstrog, R., Hassager, O., *Dynamics of Polymeric Liquids*, vol. I, Wiley, New York 1977.

[17] Israelachvili, J., *Intermolecular and Surface Forces*, Academic Press, London 1997.

[18] Netz, R. R., Andelman, D., *Phys. Rep.* 2003, *380*, 1–95.

[19] Semenov, A. N., Bonet-Avalos, J., Johner, A., Joanny, J. F., *Macromolecules* 1996, *29*, 2179–2196.

[20] Dobrynin, A. V., Obukhov, S. P., Rubinstein, M., *Macromolecules* 1999, *32*, 5689–5700.

[21] Tuinier, R., Taniguchi, T., *J. Phys. Condens. Matter* 2005, *17*, L9–L14.

[22] Parida, S. K., Dash, S., Patel, S., Mishra, B. K., *Adv. Colloid Interface Sci.* 2006, *121*, 77–110.

[23] Degré, G., Joseph, P., Tabeling, P., Lerouge, S. *et al.*, *Appl. Phys. Lett.* 2006, *89*, 024104-1–024104-3.

[24] Barnes, H. A., *J. Non-Newtonian Fluid Mech.* 1995, *56*, 221–251.

[25] Berli, C. L. A., Piaggio, M. V., Deiber, J. A., *Electrophoresis* 2003, *24*, 1587–1595.

[26] Kirby, B. J., Hasselbrink, E. F., Jr., *Electrophoresis* 2004, *25*, 187–202.

[27] Otevřel, M., Klepárník, K., *Electrophoresis* 2002, *23*, 3574–3582.

[28] Schure, M. R., Lenhoff, A. M., *Anal. Chem.* 1993, *65*, 3024–3037.

[29] Zhukov, M. Y., Ermakov, S. V., Righetti, P. G., *J. Chromatogr. A* 1997, *766*, 171–185.

[30] Ghosal, S., *Anal. Chem.* 2002, *74*, 771–775.

[31] Shariff, K., Ghosal, S., *Anal. Chim. Acta* 2004, *507*, 87–93.

[32] Ghosal, S., *Annu. Rev. Fluid Mech.* 2006, *38*, 309–338.

[33] Potoček, B., Gas, B., Kenndler, E., Štědrý, M., *J. Chromatogr. A* 1995, *709*, 51–62.

[34] Ohshima, H., *Adv. Colloid Interface Sci.* 1995, *62*, 189–235.

[35] Cohen, J. A., Khorosheva, V. A., *Colloids Surf. A Physicochem. Eng. Asp.* 2001, *195*, 113–127.

[36] Duval, J. F. L., *Langmuir* 2005, *21*, 3247–3258.

[37] Boonsong, K., Caulum, M. M., Dressen, B. M., Chailapakul, O. *et al.*, *Electrophoresis* 2008, *29*, 3128–3134.

[38] Nishi, H., Kuwahara, Y., *J. Pharm. Biomed. Anal.* 2002, *27*, 577–585.

[39] Hoogendam, C. W., de Keizer, A., Cohen Stuart, M. A., Bijsterbosch, B. H. *et al.*, *Macromolecules* 1998, *31*, 6297–6309.

[40] Wang, J., Somasundaran, P., *J. Colloid Interface Sci.* 2005, *291*, 75–83.

[41] Kulicke, W.-M., Kull, A. H., Kull, W., Thielking, H. *et al.*, *Polymer* 1996, *37*, 2723–2731.

[42] Rice, C. L., Whitehead, R., *J. Phys. Chem.* 1965, *69*, 4017–4024.

8. Appendix A

EOF of PL fluids with uniform polymer concentration

Following the constraints given in Section 3.1, the electroosmotic velocity of PL fluids is derived from Eq. (3), after including $\partial(p-\rho g_z z)/\partial z = 0$ (no pressure gradients), $E = -\partial V/\partial z$, σ_{rz} from Eq. (4), and ρ_e from Eq. (2). That is,

$$0 = \frac{\beta}{r}\frac{\partial}{\partial r}\left(r\left|\frac{\partial u_z}{\partial r}\right|^{\alpha-1}\frac{\partial u_z}{\partial r}\right) - \frac{\varepsilon}{r}\frac{\partial}{\partial r}\left(r\frac{\partial \psi}{\partial r}\right)E \tag{A1}$$

The boundary conditions required to attain $u_z(r)$ from Eq. (A1) are written as follows:

$$r = 0,\ \ \partial u_z/\partial r = 0,\ \ \partial\psi/\partial r = 0 \tag{A2}$$

$$r = R,\ \ u_z = 0,\ \ \psi = \zeta \tag{A3}$$

The first condition is a consequence of the symmetry of the flow in the cylindrical geometry. The second condition expresses the no-slip of the fluid at the wall, where $\psi(R)$ is identified as the electrokinetic ζ-potential [3]. Integrating Eq. (A1) and using Eq. (A2) yield

$$-u_z(r) = \left(\frac{\varepsilon E}{\beta}\right)^{1/\alpha}\int\left(-\frac{\partial\psi}{\partial r}\right)^{1/\alpha}\mathrm{d}r + C \tag{A4}$$

where C is an integration constant to be determined with Eq. (A3). The remaining integral cannot be worked out straightforwardly for arbitrary functions $\psi(r)$ and exponents $1/\alpha$. To proceed further, here we introduce an explicit function $\psi(r)$ that appropriately represents the EDL potential.

It is evident that such a function should be obtained by solving Eq. (2) in the flow domain of cylindrical channels, which yields an expression in terms of modified Bessel functions [42] (see [5, 6] for slit microchannels). For the sake of simplicity, here we consider $\lambda \ll R$, which is usual in practice, provided fluids with moderate ionic concentrations in micro-scale channels are considered. This condition implies both a roughly flat EDL and that EDL potentials from opposite sides of the channel do not interfere each other. Therefore, for relatively low surface potentials ($|\zeta| < 50$ mV), the Debye–Hückel approximation yields [1, 2]

$$\psi(r) = \zeta \exp[-(R-r)/\lambda] \tag{A5}$$

Finally, substituting Eq. (A5) into Eq. (A4), performing the integration, and then using Eq. (A3), leads to the following expression:

$$u_z(r) = \left(-\frac{\varepsilon\zeta E}{\beta}\right)^{1/\alpha} \frac{\alpha}{\lambda^{1/\alpha-1}} \left[1 - \exp\left(-\frac{(R-r)}{\alpha\lambda}\right)\right] \tag{A6}$$

which gives the fluid velocity profile in the capillary. The electroosmotic velocity $u^{(e)}$ is defined as the cross-sectional area average of $u_z(r)$. Because $\lambda \ll R$, the exponential term vanishes at short distances beyond the EDL region, and the fluid velocity is uniform throughout the flow domain (except in the close vicinity of the interface). Hence the electroosmotic velocity for PL solutions with uniform polymer concentration is given by

$$u_{\mathrm{U}}^{(e)} = \left(-\frac{\varepsilon\zeta E}{\beta}\right)^{1/\alpha} \frac{\alpha}{\lambda^{1/\alpha-1}} \tag{A7}$$

It should be noted that the numerical value in the bracket of Eq. (A7) must be positive: the EOF is established in the positive z-direction of the capillary for either negatively charged surfaces under positive electric field, or positively charged surfaces under negative electric field.

9. Appendix B

EOF of PL fluids with polymer depletion at the wall

On the base of the arguments given in Section 3.3, the flow domain is divided in two regions: the bulk fluid and the depletion layer (further details on this formulation are given in [11]). Thus, Eq. (3) is expressed as follows, after including $\partial(p - \rho g_z z)/\partial z = 0$ (no pressure gradients), $E = -\partial V/\partial z$, σ_{rz} from Eq. (4), and ρ_e from Eq. (2),

$$0 = \frac{\beta}{r}\frac{\partial}{\partial r}\left(r\left|\frac{\partial u_z}{\partial r}\right|^{\alpha-1}\frac{\partial u_z}{\partial r}\right), \quad 0 \le r \le (R - \delta_{\mathrm{D}}) \tag{B1}$$

$$0 = \frac{\beta_{\mathrm{D}}}{r}\frac{\partial}{\partial r}\left(r\left|\frac{\partial u_z}{\partial r}\right|^{\alpha_{\mathrm{D}}-1}\frac{\partial u_z}{\partial r}\right) - \frac{\varepsilon}{r}\frac{\partial}{\partial r}\left(r\frac{\partial\psi}{\partial r}\right)E \quad (R - \delta_{\mathrm{D}}) \le r \le R \tag{B2}$$

There are no electrical forces on the bulk fluid ($\rho_e \approx 0$ in Eq. (B1)) because the EDL potential is assumed to vanish in the depletion layer, which requires $\lambda \ll \delta_{\mathrm{D}}$. The parameters of the PL model in the depletion layer (Eq. (B2)) are different from those in the bulk. In addition, boundary conditions are

$$r = 0, \quad \sigma_{rz} = 0 \tag{B3}$$

$$r = R - \delta_{\mathrm{D}}, \quad \sigma_{rz}^{(\mathrm{bulk})} = \sigma_{rz}^{(\mathrm{depl})}, \quad u_z^{(\mathrm{bulk})} = u_z^{(\mathrm{depl})}, \quad \partial\psi/\partial r = \psi = 0 \tag{B4}$$

$$r = R, \quad u_z = 0, \quad \psi = \zeta \tag{B5}$$

Equation (B3) is due to the symmetry of the cylindrical geometry. Equation (B4) establishes the matching of shear stresses and fluid velocities at the surface connecting both regions. Equation (B5) is the no-slip condition at the wall, where $\psi(R)$ is assumed to be the ζ-potential.

Integrating Eqs. (B1) and (B2), using boundary conditions (B3)–(B5), and including $\psi(r)$ from Eq. (A5), leads to the following expression of the electroosmotic velocity:

$$u_z(r) = \left(-\frac{\varepsilon\zeta E}{\beta_{\mathrm{D}}}\right)^{1/\alpha_{\mathrm{D}}} \frac{\alpha_{\mathrm{D}}}{\lambda^{1/\alpha_{\mathrm{D}}-1}} \left[1 - \exp\left(-\frac{(R-r)}{\alpha\lambda}\right)\right] \tag{B6}$$

It is observed that the EOF is completely defined in the depletion layer, and the central region is simply transported as a plug. Of course, this is valid for $\lambda \ll \delta_{\mathrm{D}}$. Finally, the electroosmotic velocity for polymer solutions with depletion at the wall is

$$u_{\mathrm{D}}^{(\mathrm{e})} = \left(-\frac{\varepsilon\zeta E}{\beta_{\mathrm{D}}}\right)^{1/\alpha_{\mathrm{D}}} \frac{\alpha_{\mathrm{D}}}{\lambda^{1/\alpha_{\mathrm{D}}-1}} \tag{B7}$$

where α_{D} are β_{D} are the parameters of the PL model characterizing the viscosity of the depletion layer (not the bulk solution).

